Journal of Non-Crystalline Solids 354 (2008) 3773–3779

Contents lists available at ScienceDirect

Journal of Non-Crystalline Solids

journal homepage: www.elsevier.com/locate/jnoncrysol

Influence of metal organic and inorganic precursors on spray pyrolyzed ceramic MgO (200) thin films for epitaxial over layers

A.M. Ezhil Raj [b], K. Vijayalakshmi [d], G. Selvan [e], M. Jayachandran [c], C. Sanjeeviraja [a,*]

[a] Department of Physics, Alagappa University, Karaikudi 630 003, India
[b] Department of Physics, Scott Christian College (Autonomous), Nagarcoil 629 003, India
[c] ECMS Division, Central Electrochemical Research Institute, Karaikudi 630 006, India
[d] Department of Physics, Bishop Heber College, Tiruchirapalli 620 017, India
[e] Department of Physics, Thanthai Hans Roever College, Perambalur 621 212, India

ARTICLE INFO

Article history:
Received 30 October 2007
Received in revised form 20 February 2008
Available online 2 May 2008

PACS:
77.55.+f
81.70.Pg
61.10.Nz
78.66.Qn
68.37.Hk
68.37.Ps

Keywords:
Ceramics
Heavy metal oxides
Atomic force and scanning tunneling microscopy
Scanning electron microscopy
FT-IR measurements
X-ray diffraction

ABSTRACT

The MgO (200) surface is widely used as a substrate for epitaxial growth of superconducting and ferro-electric films. Highly oriented, single crystalline, extremely flat and transparent MgO films have been successfully deposited on quartz substrates by the chemical spray pyrolysis technique using economically viable metal organic and inorganic precursors under optimized conditions at the substrate temperature of 600 °C. Thermal analysis (TGA/DTA) in the temperature range 30–600 °C with the heating rate of 10 °C/min revealed the decomposition behavior of the precursors and confirmed the suitable substrate temperature range for film processing. The heat of reaction, ΔH due to decomposition of metal organic precursor contributed additional heat energy to the substrate for better crystallization. The intensity of the (200) peak in X-ray diffraction (XRD) measurements and the smooth surface profiles revealed the dependency of precursor on film formation. The compositional purity and the metal–oxide bond formation were tested for all the films. UV–Vis–NIR optical absorption in the 200–1500 nm range revealed an optical transmittance above 80% and the absorption edge at about 238 nm corresponding to an optical band gap E_g = 5.25 eV. Scanning electron microscopy (SEM) and atomic force microscopy (AFM) micrographs of MgO films confirmed better crystallinity with larger grain size (0.85 μm) and reduced surface roughness (26 nm), respectively.

1. Introduction

The refractory oxide magnesia finds many attractive applications in diverse fields. Most of the existing qualities of MgO like ionic conductivity, thermal and chemical stability make these films useful as a buffer layer for depositing ferro-electric and superconducting films on various substrates because of the lattice matching (0.4212 nm) of majority of overlaying films. Among the available planes of the MgO lattice, the (200) surface has been subjected to numerous studies because it finds many applications in the epitaxial growth of metals [1–4] and superconductors [5–7]. Since MgO crystallizes in NaCl structure with fcc lattice (space group *Fm*3*m*), it can be easily synthesized along (200) plane, for which surface energy is much lower than any other orientations [8]. Recently, MgO films have been implemented as a protective dielectric coating in plasma display panels (PDPs) [9,10]. It was reported that the performance of the MgO protective layer also depends on the preferred orientation of the film [11]. Unfortunately, bulk MgO crystal substrates are often imperfect due to their quality and subsequently the films grown on their surfaces can be affected by surface roughness, miscut, distribution of domains and curvature [12]. These problems can easily be solved by replacing single crystal substrates with highly oriented (200) MgO thin films.

During the last few decades, several preparation methods for MgO films have been reported such as pulsed laser deposition [13], magnetron sputtering [14], chemical vapor deposition [15], chemical spray pyrolysis [16] and electron beam evaporation [17]. Among these, the chemical spray pyrolysis method has several advantages over other methods such as relatively low cost, easy composition control, large area deposition and the higher growth rate. Recently, the spray pyrolysis method emerged as a

* Corresponding author. Tel.: +91 04565 230251; fax: +91 04565 225202.
E-mail address: sanjeeviraja@rediffmail.com (C. Sanjeeviraja).

0022-3093/$ - see front matter © 2008 Elsevier B.V. All rights reserved.
doi:10.1016/j.jnoncrysol.2008.03.043

viable deposition process capable of producing nano-sized particles of oxide and sulfide materials, very receptive to heat treatment and pyrolysis [18,19].

Even though MgO ceramic layers have been grown on different substrates by using various precursors, the effect of precursors on the growth of oriented films on quartz substrate has not been reported in detail and compared in the context of the spray pyrolysis process. Since the effects of the lattice matching across the film/substrate interface are excluded, the film growth on amorphous substrates may give us substantial information about the growth characteristics of the MgO crystal lattice itself. The main objective of the present study is to prepare MgO films with (200) preferred orientation by using economically viable magnesium acetate, magnesium nitrate, and magnesium chloride as the starting materials, and by spraying through a simple aerosol spray nozzle onto quartz substrates.

2. Experiment

In the present work, a downward spraying system was used to deposit MgO thin films using different metal organic/inorganic precursors. The starting materials used for thin film preparation, their concentration and all other related parameters are given in Table 1. The precursor solution was prepared by sol–gel processing of the salts, in ethanol separately using an acid catalyst to stable the solutions. Ethanol was used as the principal solvent and triethyleneglycol (TEG) was added as an additional solvent to facilitate high temperature processing [20]. Precursor flow rate was controlled with an adjusting valve and filtered air was administered as carrier gas whose flow rate was monitored with a flow meter. The substrate was positioned on a stainless steel platform of the furnace and heated to desired temperature up to a maximum of 1000 °C. The distance between the spray nozzle and substrate was set at an optimized value of 30 cm. An atomizer was kept above the substrate to obtain a soft, low-velocity spray and uniform distribution of micronized droplets (Fig. 1). The optimized deposition parameters for the preparation of MgO thin films in the present study are summarized in Table 1. Prior to deposition, the quartz substrates of size 10 mm × 25 mm were initially cleaned with hot chromic acid and then rinsed, respectively with acetone, methanol and propane-2-ol. Finally they were ultrasonically cleaned in deionized water. MgO films were prepared in a temperature controlled tubular furnace, where temperature can be controlled to an accuracy of ±0.1 °C.

All the depositions were carried out in atmospheric air. The film thickness was measured using Stylus profiler (Mitutoyo SJ-301). The deposition rate was estimated from the deposition time and the thickness of the film. Typical deposition rate of MgO films were between 40 and 50 nm/min for the precursor flow rate of 5 ml/min.

Table 1
Starting precursors and optimized deposition conditions for the preparation of MgO thin films

Spray parameters	Values
Starting precursors	$Mg(CH_3COO)_2 \cdot 4H_2O$ $Mg(NO_3)_2 \cdot 6H_2O$ $MgCl_2 \cdot 6H_2O$
Precursor concentration	0.15 M
Precursor volume	50 ml
Substrate	Quartz
Substrate temperature	600 °C
Solution feeding rate	5 ml/min
Carrier gas pressure	0.4 kg/cm^2
Solvent	95% Ethanol with TEG
Nozzle-substrate distance	30 cm
Deposition time	10 min

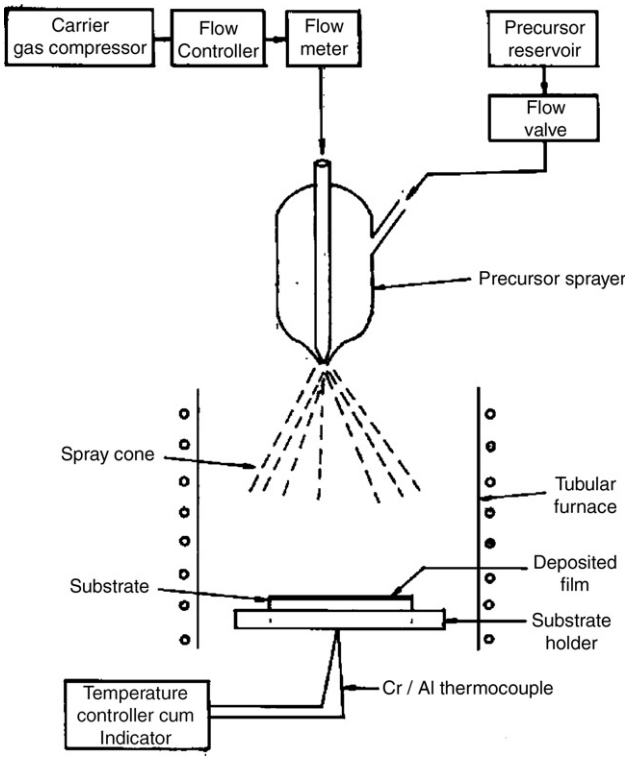

Fig. 1. Spray pyrolysis set-up.

The thermal stability, constituent composition of each precursor and the compounds formed at various transition regions were analyzed using the thermogravimetry analysis (TGA) and differential thermal analysis (DTA) [Perkin Elmer, Diamond]. The effect of precursor on the preferentially oriented growth of MgO films was studied on X-ray diffractometer (X'pert Pro) using the Cu Kα radiation. From the full width at half maximum (FWHM) of the XRD peaks, the average grain size in the MgO film was estimated. The Mg–O bonding and vibrational modes were studied by Fourier transform infrared spectroscopy (FT-IR). The FT-IR spectra were recorded in the range of 400–4000 cm^{-1}, with spectral resolution of 4 cm^{-1}. The elemental composition of the film was analyzed using energy dispersive X-ray (EDX) spectrometer attached with the JEOL JSM-35 CF SEM instrument. Prepared films were much transparent whose transmittance behavior was analyzed at RT using the UV–Vis–NIR spectrophotometer (Hitachi-3400), and the optical band gap energy of the resulted films was estimated from the Tauc plot drawn. Surface morphology of the film was analyzed using the micrographs obtained from scanning electron microscope (JEOL JSM-35 CF) and atomic force microscope (Nanoscope-E AFM/STM).

3. Results

3.1. Thermal decomposition behavior of the precursors

Fig. 2 shows the typical thermograms of the starting precursors: (a) magnesium acetate, (b) magnesium nitrate and (c) magnesium chloride decomposed in air at atmospheric pressure. The results obtained from thermogravimetry indicates that the decomposition of all the hydrated precursors are not similar in air atmosphere in the entire temperature range studied (30–600 °C).

The TGA curve of magnesium acetate (Fig. 2(a)) is essentially a three steps process. The thermal decomposition reaction follows the stoichiometry [21]:

$$Mg(CH_3COO)_2 \cdot 4H_2O \rightarrow Mg(CH_3COO)_2 + 4H_2O,$$

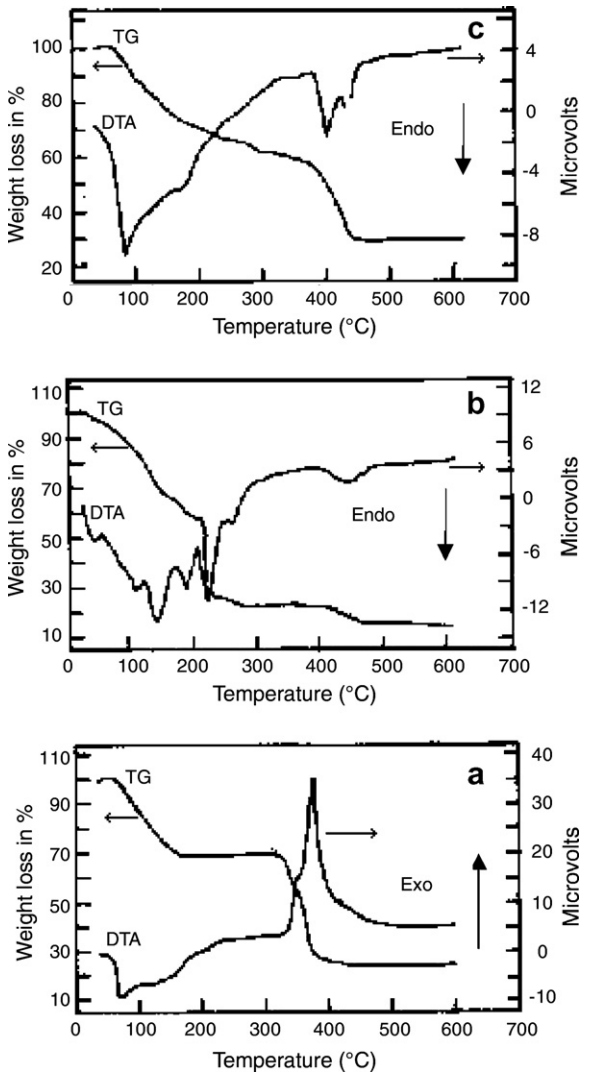

Fig. 2. TGA/DTA thermograms of the starting precursors: (a) magnesium acetate (b) magnesium nitrate and (c) magnesium chloride.

$$Mg(CH_3COO)_2 \rightarrow MgCO_3 + (CH_3)_2 \cdot CO,$$

$$MgCO_3 \rightarrow MgO + CO_2.$$

The first mass loss occurs over the temperature range 61–168 °C; the mass loss of 31.64% is slightly less than the loss of four moles of water per mole of salt (33.60%). The second stage begins at about 168 °C, proceeded slowly up to 346 °C, and then the reaction became extremely rapid, leading to a final loss of 40% releasing acetone in vapor phase. This value is nearly same as that predicted for the formation of crystalline magnesium oxide due to the decomposition of magnesium carbonate releasing carbon dioxide.

The mass loss curve of $Mg(NO_3)_2 \cdot 6H_2O$ is illustrated in Fig. 2(b). The decomposition mechanism leads to the liberation of NO_2 in gaseous phase according to the reaction:

$$2[Mg(NO_3)_2 \cdot 6H_2O] \rightarrow 2MgO + 4NO_2 + 12H_2O.$$

DTA curves however are discontinuous line, and subtle mass changes are emphasized in which minor reactions occur during or near a major reaction. On the other hand, similar curves for $MgCl_2 \cdot 6H_2O$ are shown in Fig. 2(c). The decay mechanism of the precursor released HCl gaseous product according to the reaction:

$$MgCl_2 \cdot 6H_2O \rightarrow MgO + 2HCl + 5H_2O.$$

As seen, water of hydration is not removed completely, only five moles of water is evolved and the remaining water reacts with the precursor and produces intermediate compound and so subtle mass changes are seen in the thermogram. Reaction with one mole of water is revealed as,

$$MgCl_2 + H_2O \rightarrow Mg(OH)Cl + HCl,$$

$$Mg(OH)Cl \rightarrow MgO + HCl.$$

Due to this reaction of precursor with water, additional inflection points are seen in the thermogram.

The decomposition temperature of the anhydrous salts to magnesium oxide was different and this may be due to the marked deviations in this physico-chemical and material properties, especially due to the melting point of 323, 95, 180 °C for the acetate, nitrate and chloride salts respectively. Because of low melting point, the nitrate and chloride salts react with water during dehydration and resulted in the formation of new intermediate compounds. These intermittent compounds on absorbing heat, then decomposed during transformation showing more endothermic peaks, and hence no horizontal mass loss level is observed in these thermograms. However, the acetate salt having high melting point 323 °C, after dehydration, exhibits a horizontal mass loss region followed by a sharp exothermic peak marking a heat evolved decomposition process at 343 °C leading to the formation of MgO.

Integration of the area under a DTA curve provides a direct measurement of the change in enthalpy (ΔH) of the sample for a thermally induced transition [22] according to the equation,

$$A = -km\Delta H, \quad (1)$$

where 'A' is the area under an exothermic/endothermic peak, 'k' is the instrumental constant, 'm' is the mass of the sample and 'ΔH' is the change in enthalpy of reaction. For the same sample mass, in nitrate and chloride samples, the broad endotherms with a negative change in heat capacity is an indication of non-crystalline rearrangements, fusion or solid state transitions for the relatively impure residue, magnesium oxide. This has been further confirmed by the 'second order or glass' transition observed as a base line shift, which denotes some disorder within the system. The exothermic/endothermic heat exchanges during decompositions are indicated by arrow marks in Fig. 2. However, the acetate salt exhibits narrow exotherm with less glass transition, which accelerates crystallization leading to a stable system. These arguments are explicitly supported by the enthalpy values calculated as −641.8, −189.9 and +1741.77 kJ/mol from the endothermic and exothermic peaks observed for the $MgCl_2 \cdot 6H_2O$, $MgNO_3 \cdot 6H_2O$ and $Mg(CH_3COO)_2 \cdot 4H_2O$ precursors, respectively.

3.2. X-ray diffraction analysis

Fig. 3 shows the typical X-ray diffraction patterns of the MgO films prepared from the acetate (a), nitrate (b) and chloride (c) precursors, keeping the deposition parameter constant as given in Table 1. X-ray diffraction pattern of the MgO powder sample is also given for comparison. Regarding the MgO films prepared from acetate and nitrate precursors, they show crystalline nature and their crystallization is almost preferentially oriented along (200) direction. Moreover, the intensity of MgO (200) peak obtained from the acetate precursor is high compared to the peak intensity of the film prepared from the nitrate precursor. The films obtained from the chloride precursors were nearly amorphous due to the intermittent reactions, which produced additional compounds as it readily reacts with water under normal atmosphere conditions. The crystallite size was determined using Scherrer formula [19], by measuring the FWHM of the (200) peak

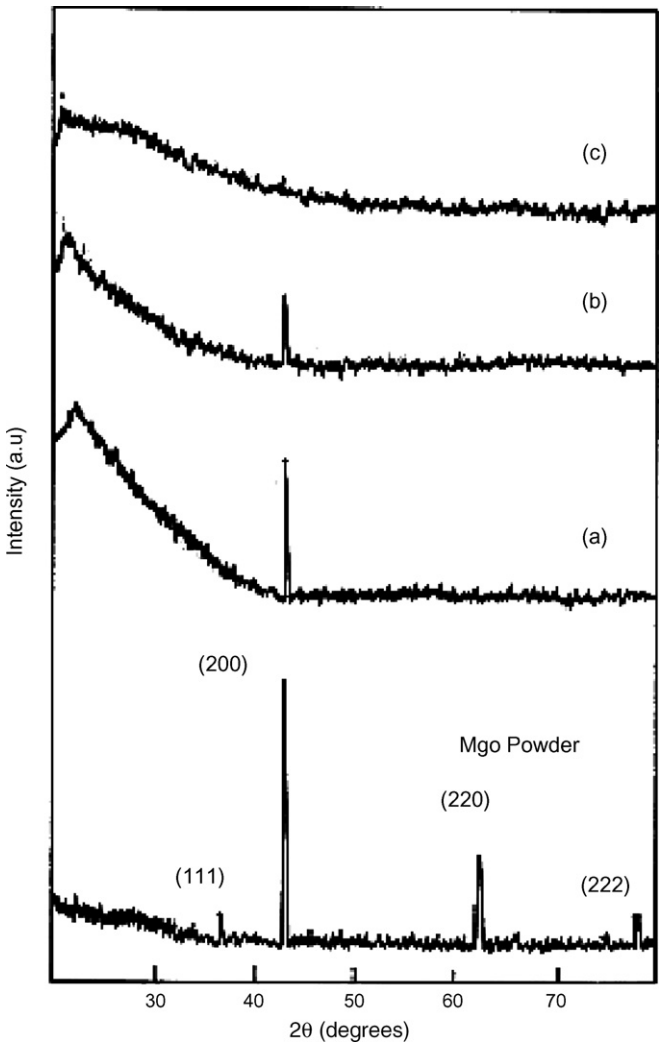

Fig. 3. XRD pattern of the sprayed MgO films derived from the precursors: (a) magnesium acetate, (b) magnesium nitrate and (c) magnesium chloride.

$$D = \frac{K\lambda}{\cos\theta\sqrt{\beta^2 - \beta_0^2}}, \tag{2}$$

where $K = 0.94$, λ is the wavelength of incident X-ray radiation (1.542 Å for Cu Kα), β the intrinsic full width at half maximum of peak, β_0 the integral peak width caused by instrumental broadening and θ is the Bragg's diffraction angle of the respective XRD peak.

3.3. FT-IR and composition analysis

Fourier transform IR spectra were recorded for all the MgO thin films prepared from the three precursors in the range 400–4000 cm^{-1}. Fig. 4(a)–(c) shows the FT-IR spectra of the MgO films deposited from the acetate, nitrate and chloride precursors. The spectrum pertaining to MgO film prepared from acetate precursor (Fig. 4(a)) shows that the band appearing at ~3634 cm^{-1} of the as-deposited film reveals the presence of the weakly hydrogen bonded hydroxide ions (due to the γ (OH) mode) [23,24]. The peak at 1228 cm^{-1} is assigned to the deformation band in water. These bands are due to hydration, originated from the precursor and solvent or from exposure to the atmosphere. It is well known that H_2O molecules are chemisorbed onto the film surfaces when exposed to the atmosphere. Therefore, a small amount of impurity is likely to be incorporated in the film during its exposure to atmospheric ambient. The appearance of the two strong bands due to the γ (Mg–O) mode at 533 and 485 cm^{-1} in the FT-IR spectra is a clear evidence for the presence of crystalline MgO. This implies that the MgO films prepared using acetate precursor is nearly stoichiometric and consist of traces of hydration. Similar observations on the MgO films prepared using the nitrate and chloride precursors (Fig. 4(b) and (c), respectively), showed strong and additional bands due to impurities that aroused due to the intermittent reaction of the compound during decomposition. Moreover, the FWHM of the peak at 485 cm^{-1} of the acetate-derived film is narrow; showing narrow distribution of vibrational energy. This in turn indicates the increase in crystallinity with larger grain size [25], which is already confirmed through the XRD results.

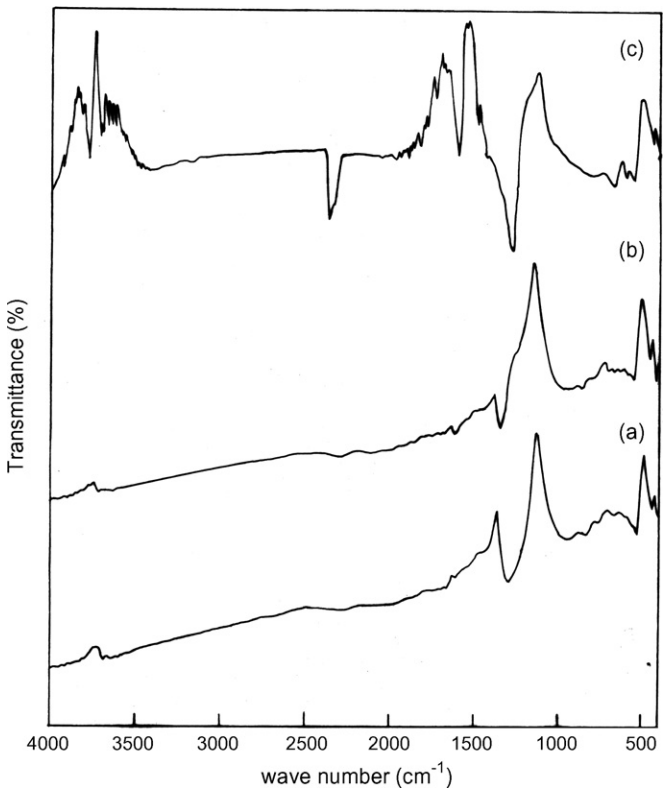

Fig. 4. FT-IR spectrum of the MgO film derived from (a) magnesium acetate precursor, (b) magnesium nitrate and (c) magnesium chloride precursors.

In support of this FT-IR observation, the EDX spectrum (Fig. 5) of stoichiometric MgO surface prepared at 600 °C on the quartz substrate using the acetate precursor shows only the magnesium and oxygen peaks appear at the positions with the binding energy 1.27 and 0.54 keV, respectively. The atomic percentage of Mg and O present in the film are calculated and are found to be 1.00:1.03 showing perfect stoichiometry of the film surface. This result is far better than that derived for the MgO films deposited from the nitrate and chloride precursors.

3.4. Optical transmittance and band gap

The study of optical properties was done based on the experimental transmittance measurements [26] of the MgO films deposited using the three starting precursors. It is observed from Fig. 6 that the MgO films deposited using acetate precursor exhibits sufficiently high transmittance above 80%, where as the films prepared with nitrate and chloride precursors have less transmittance. The functional dependence of $(\alpha h\nu)^2$ vs. $h\nu$ for the insulator films is accessible to measure the optical band gap. It is known that for a large number of semiconductor/insulator thin films in crystalline or amorphous form, the dependence of absorption

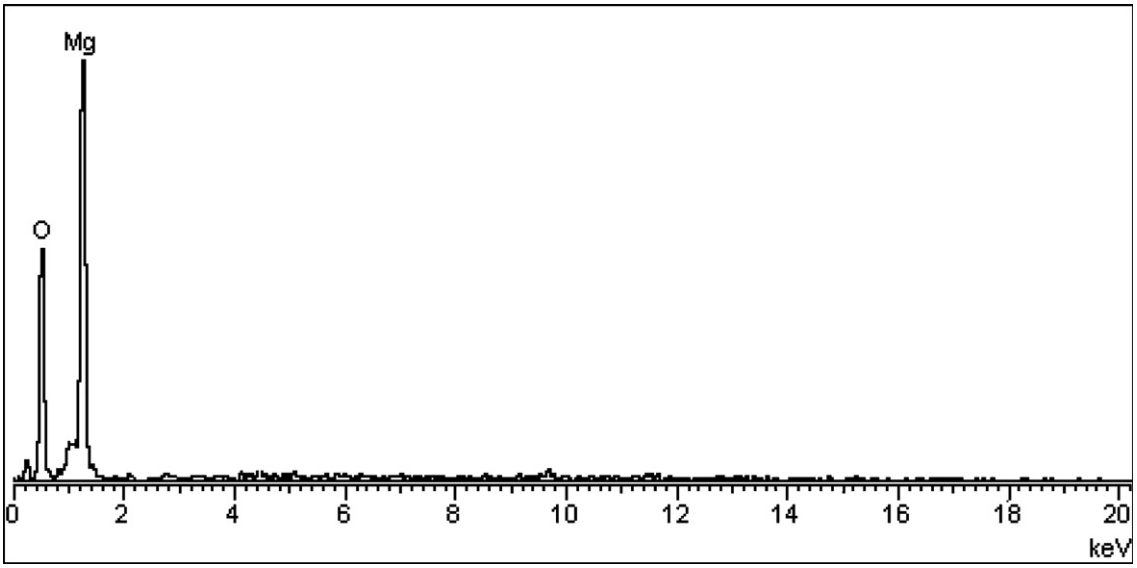

Fig. 5. EDAX spectrum of MgO films deposited using acetate precursor at 600 °C.

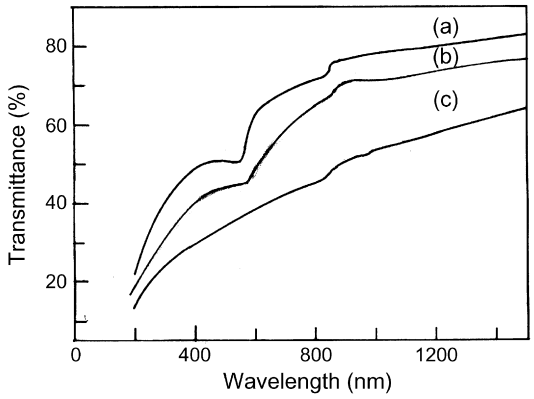

Fig. 6. Optical transmittance spectra of MgO films prepared from (a) acetate (b) nitrate and (c) chloride precursors.

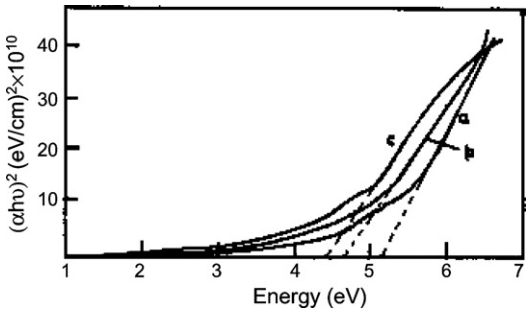

Fig. 7. $(\alpha h\upsilon)^2$ vs. $h\upsilon$ curves of MgO films prepared from (a) acetate (b) nitrate and (c) chloride precursors (dotted line curves provide the optical band gap energy directly).

co-efficient 'α' upon the photon energy $h\nu$ for optically induced transitions takes the form,

$$\alpha h\nu = A(h\nu - E_g)^n, \tag{3}$$

where 'E_g' is the optical band gap, 'A' is a constant, and '$h\nu$' is the photon energy, while 'n' depends on the nature of the transition.

For direct transitions, $n = 1/2$ or $3/2$, while for indirect ones $n = 2$ or 3, depending on whether they are allowed or forbidden respectively. The dependence of $(\alpha h\nu)^2$ on the photon energy should result in a straight line intercepting the abscissa at $h\nu = E_g$ [27]. In our case, the best linear fit of $(\alpha h\nu)^2$ vs. $h\nu$ was obtained for $n = 1/2$ as shown in Fig. 7. This exponent $n = 1/2$, indicates that the obtained MgO thin films are wide band gap insulators with allowed direct transitions. The calculated optical band gap value 'E_g' is 5.25 eV for the acetate-derived MgO film, which is obviously much less compared with the bulk value (>7 eV). MgO films deposited from the nitrate and chloride salts exhibited lower band gap values of 4.68 and 4.45 eV, respectively. However, the transmittance values of these films are very low, about 65% and 55%, respectively.

3.5. Surface morphology and microstructure

SEM observations show the surface morphology of MgO thin films that correlates the profound changes with the starting precursors. Films prepared using magnesium acetate has a uniform surface morphology with square/rectangular grain like structures over the surface (Fig. 8(a)). The average grain size of about 0.85 μm with out the usual cracking behavior associated with spray pyrolysis revealed the good quality of the films compared to the MgO films prepared with other precursors (Fig. 8(b) and (c)). The peak to peak roughness is only in the range between 1500 Å and 2000 Å. Optical transparency is therefore higher in the films deposited with magnesium acetate precursor.

Further, Fig. 9 shows the AFM images of MgO thin films synthesized from three different starting precursors. AFM images resolved the nano-size particulate microstructure of the films. Fig. 9(a) shows that, MgO films prepared from acetate precursor nucleated as individual spherical islands, which shows near atomically flat terraces with low step density. The RMS roughness of the film surfaces are calculated relative to the least-square fitted line of the surface profile. It is expressed in an equation as,

$$\text{RMS roughness} = \text{Sqrt}\left[\frac{1}{N_L}\sum_{i=1}^{N_L} Z_i^2(x)\right], \tag{4}$$

where 'N_L' is the number of discrete measurement points on the profile and '$Z(x)$' is the height deviation of the profile from a least-square fitted line.

RMS roughness values were determined (nanoscope III, DI software) for all the films and are found to influence by the use of precursors. The RMS roughness of the acetate-derived MgO thin film

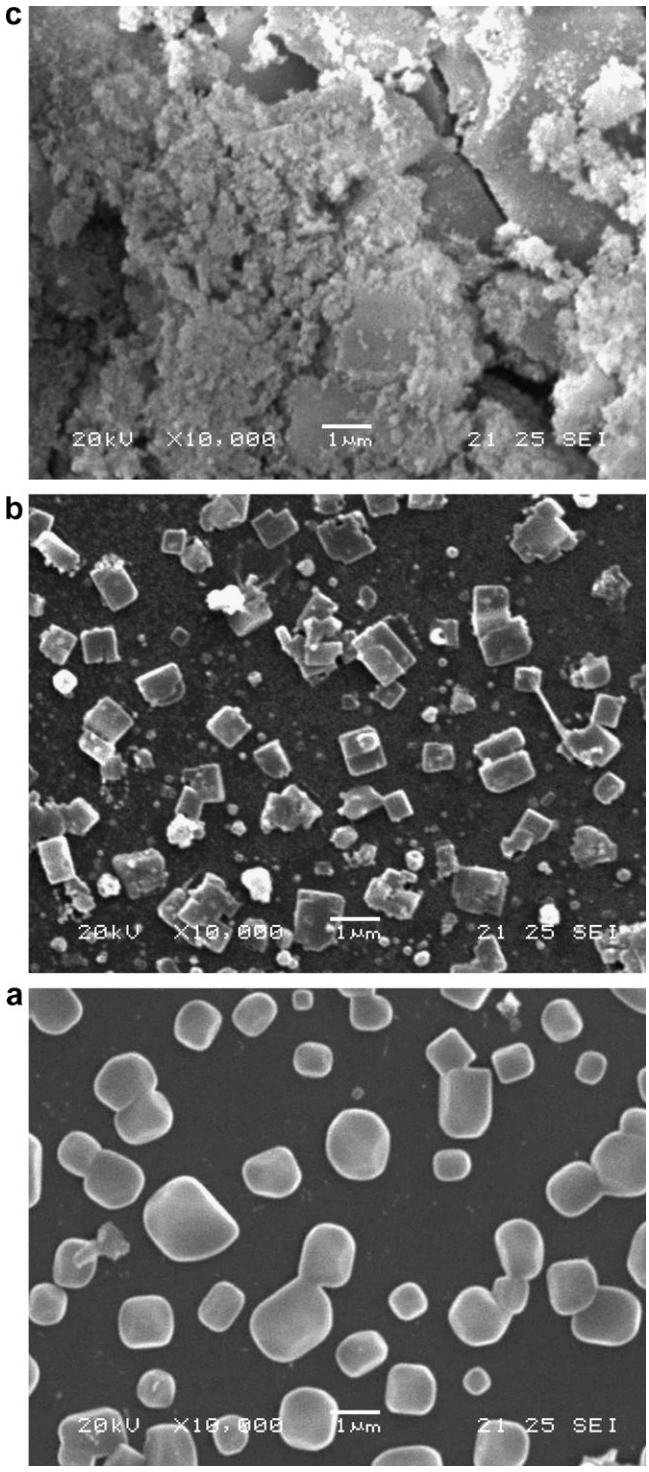

Fig. 8. SEM Micrographs of MgO film processed from (a) acetate (b) nitrate and (c) chloride precursors.

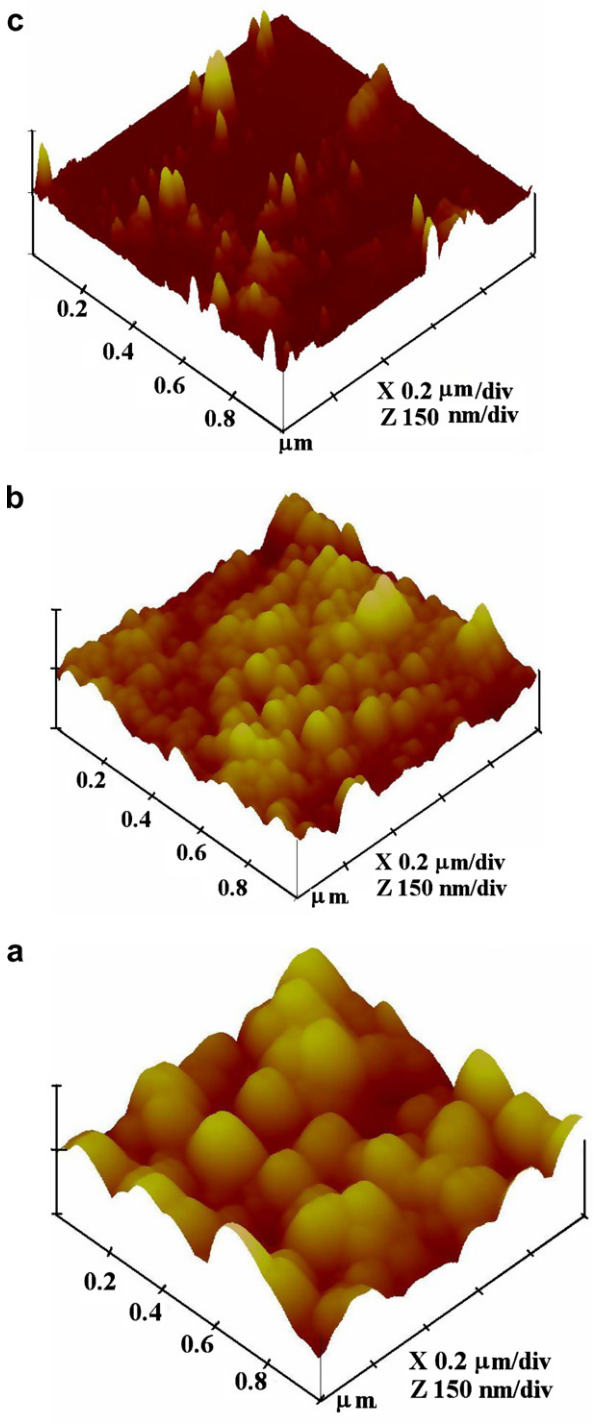

Fig. 9. AFM images of MgO surfaces prepared with (a) acetate (b) nitrate and (c) chloride precursors at 600 °C.

surface is about 26 nm, meaning that the MgO films grown are flatter and parallel to the quartz substrate surface. AFM images of the MgO surface attained from other precursors (Fig. 9(b) and (c)) appear granular with irregularly shaped grains and therefore had comparatively large surface roughness, 37 nm and 48 nm for the nitrate and chloride precursor, respectively. Also it is evident that the grain size of the acetate-derived film is higher than that of the films prepared from chloride and nitrate precursors. These observations are consistent with the results of the XRD and FT-IR studies.

4. Discussion

In order to identify a suitable precursor for preparing preferentially oriented single crystalline MgO thin films, the chemical processes involved during the transformation from metal organic/inorganic compound to metal oxide have been investigated from the recorded thermograms (TGA/DTA) in air atmosphere. From the observed weight loss and the heat flow processes associated with the different chemical transformations occurring during the transition to metal oxide, it is evident that the thermogravimetric

behaviors of the three starting materials chosen in the present study are entirely different from each other. According to various theories on DTA [28–30], the area under the exothermic or endothermic peak is proportional to the heat of reaction or transition and the mass of reactive sample. Comparatively, acetate precursor has large area exotherm with less glass transition, an indicative of possible crystalline rearrangements. This observation suggests that the reaction is complete in all respect leading to the formation of the expected final stoichiometric oxide compounds. In addition, the exothermic feature serves as a means of qualitative identification of the substance, where the sample temperature leads the reference temperature because of the exothermic heat evolved from the sample. These observations clearly indicate that magnesium acetate could be a suitable precursor for the preparation of magnesium oxide thin films than the other two precursors.

The observed sharp peak in the MgO film prepared from acetate precursor may be attributed to the exothermic reaction that triggers the decomposition of the precursor which provided the required quantity of heat energy leading to a complete crystallization as evidenced from the TG/DTA plots and the formation of stoichiometric metal oxide.

It is interesting to note that the crystallite size of MgO films obtained from the acetate precursor was larger (52 nm) than the film prepared from nitrate precursor (41 nm). This increased crystalline nature and crystallite size might have been associated with the exothermic reaction observed in acetate precursor as evident from the (200) XRD peak whose intensity is high and width is narrow.

The observed two strong bands of γ (Mg–O) mode in the FT-IR spectra confirm the formation of stoichiometric MgO films which is further supported by the EDAX analysis as well. The observed change of the optical band gap with precursors can be explained on the basis of the density of states model proposed by Mott and Davis [31]. Accordingly, the width of the localized states near the mobility edges depends on the degree of disorder and defects present in the deposited MgO films. The presence of a high concentration of localized states in the band structure of less crystalline and amorphous films is responsible for the low values of energy gap. The reduction in the number of defects in the well crystallized MgO film prepared from acetate precursor, decreases the density of localized states in its band structure, consequently increasing its optical band gap to a maximum value of 5.25 eV.

It is inferred from the SEM images that the surface quality is highly dependent on the nature of precursor. AFM studies on surface morphology also support this and the grain size variation is consistent with the crystallite size variation observed from XRD peak analysis.

5. Conclusions

Magnesium oxide films were prepared by the spray pyrolysis technique using various types of metal organic/inorganic precursors as the starting material. Though the films prepared from acetate and nitrate precursors exhibited, the same typical cubic structures for the MgO compound, (200) peak intensity of the samples derived from nitrate precursor was less compared to the acetate samples. These variations were reflected in the grain size measurement, which shows that fully crystallized and highly oriented film formation is favored when acetate precursor is used. Surface characterization revealed that the films prepared from the acetate precursors were smooth and denser accompanied with a high transmittance in the visible and near IR range of the spectrum. The optical band gap of acetate-derived film is 5.25 eV, which is higher than the values reported for other samples. It can be concluded that the microstructure of the MgO surfaces deposited using acetate precursor, revealed the (200) oriented growth of smooth surfaces of single crystalline nature without any crack that are suitable for the growth of epitaxial layers and devices.

References

[1] Y.C. Lee, P. Tong, P.A. Montano, Surf. Sci. 181 (1987) 559.
[2] C. Li, R. Wu, A.J. Freeman, C.L. Fu, Phys. Rev. B 48 (1993) 8317.
[3] P. Guénard, G. Renaud, B. Villette, Physica B 221 (1996) 205.
[4] P. Guénard, G. Renaud, B. Villette, M.H. Yang, C.P. Flynn, Scripta Metall. Mater. 31 (1994) 1221.
[5] M. Gurvitch, A.T. Fiory, Appl. Phys. Lett. 51 (1987) 1027.
[6] D.K. Fork, F.A. Ponce, J.C. Tramontana, T.H. Gabelle, Appl. Phys. Lett. 58 (1991) 2294.
[7] W.J. DeSisto, R.L. Henry, J. Cryst. Growth 109 (1991) 314.
[8] V.E. Henrich, P.A. Cox, The Surface Science of Metals Oxides, Cambridge University, Oxford, 1994.
[9] B.W. Byrun Jr., IEEE Trans. Electron Dev. 22 (1975) 685.
[10] T. Ugrade, T. Iemori, M. Osawa, N. Nakayama, I. Morita, IEEE Trans. Electron Dev. 23 (1976) 313.
[11] E.H. Choi, H.J. Oh, Y.G. Kim, Jpn. J. Appl. Phys. 37 (12B) (1998) 7015.
[12] A. Ellison, H. Radamson, M. Tuominen, S. Milita, C. Hallin, A. Henry, O. Koesin, T. Tuomi, R. Yakimova, R. Madar, E. Janzen, Diam. Relat. Mater. 6 (1997) 1368.
[13] T. Ishiguro, Y. Hiroshima, T. Inoue, Jpn. J. Appl. Phys. 33 (1996) 3557.
[14] I. Shih, S.L. Wu, L. Li, C.X. Qiu, P. Grant, M.W. Denhoff, Mater. Lett. 11 (1991) 161.
[15] Z. Lu, R.S. Feigelson, R.K. Rome, S.A. DiCorolis, R. Illitrate, R.D. Jaacowitz, J. Cryst. Growth 128 (1993) 14.
[16] X. Yi, W. Wenzhong, Q. Yitai, Y. Li, C. Shaken, Surf. Coat. Technol. 82 (1996) 291.
[17] J. Talachio, G.R. Wagner, H.C. Pohl, Physica C 162–164 (1989) 659.
[18] D. Albin, S.H. Risbud, Adv. Ceram. Mater. 2 (3A) (1987) 243.
[19] Y.M. Gao, P. Wu, J. Balliol, K. Dwight, A. Wold, Mater. Res. Bull. 24 (1989) 1215.
[20] S.H. Rhee, Y. Yang, H.S. Chi, J.M. Myoung, K. Kim, Thin Solid Films 396 (2001) 23.
[21] M.D. Judd, B.A. Plunkett, M.I. Pope, J. Therm. Anal. 6 (1974) 555.
[22] Wesley W.M. Wendlandt, Thermal Analysis, John-Wiley, 1986.
[23] M.O. Aboelfotoh, K.C. Park, W.A. Parkin, J. Appl. Phys. 48 (1977) 2910.
[24] S.G. Kim, H. Choi, J.H. Eun, H.J. Kim, C.S. Hwang, Thin Solid Films 377&378 (2000) 694.
[25] I. Wang, Y.E. Zhao, D. Chen, S.P. Wong, Nucl. Instrum. Methods Phys. Res. B 22 (2005) 82.
[26] R. Swanepoel, J. Phys. E: Sci. Instrum. 16 (1983) 1214.
[27] J. Tauc, R. Grigorovici, A. Yancu, Phys. Status Solidi 15 (1966) 627.
[28] A.W. Coats, J.P. Redfern, Nature 201 (1964) 68.
[29] L. Reich, S.S. Stivala, Thermochem. Acta 24 (1978) 9.
[30] A.E. Newkirk, Anal. Chem. 32 (1960) 558.
[31] N.F. Mott, E.A. Davis, Electronics Process in Non-crystalline Materials, Clarendon, Oxford, 1971.